Application of an Internally Consistent Material Model to Determine the Effect of Tool Edge Geometry in Orthogonal Machining

Roy J. Schimmel
e-mail: roy.schimmel@gm.com

William J. Endres
e-mail: endres@umich.edu

Dept. of Mechanical Engineering,
University of Michigan,
Ann Arbor, MI 48109-2125

Robin Stevenson
Enterprise Systems Laboratory,
General Motors R & D Center,
Warren, MI 48090-9055
e-mail: rstevenson@gmr.com

It is well known that the edge geometry of a cutting tool affects the forces measured in metal cutting. Two experimental methods have been suggested in the past to extract the ploughing (noncutting) component from the total measured force: (1) the extrapolation approach and (2) the dwell force technique. This study reports the behavior of zinc during orthogonal machining using tools of controlled edge radius. Application of both the extrapolation and dwell approaches showed that neither produces an analysis that yields a material response consistent with the known behavior of zinc. Further analysis shows that the edge geometry modifies the shear zone of the material and thereby modifies the forces. When analyzed this way, the measured force data yield the expected material response without requiring recourse to an additional ploughing component.
[DOI: 10.1115/1.1448334]

1 Introduction

The effect of cutting edge geometry has long been an issue in understanding metal cutting. In his analysis, Merchant [1] clearly indicated the assumption of tool sharpness. There is an understanding, however, that the machining force trends will be different for a sharp tool as compared to those of a blunt tool, with all else being held constant. A ''sharp tool'' is a theoretical tool that possesses an edge radius of zero, whereas a ''blunt tool'' exhibits a non-zero radius on the cutting edge. The ratio of the edge radius to the uncut chip thickness has been used by some investigators as a measure of whether or not the tool should be treated as sharp or blunt.

Many researchers have since investigated the influence of edge geometry on the cutting process. One phenomenon closely related to the effect of the edge bluntness is the apparent increase in specific energy required to form a chip as the uncut chip thickness is decreased. Backer et al. [2] were among the earliest to study this phenomenon and in doing so coined the term *size effect*. They were concerned with grinding processes, in particular the apparent approach of the work material strength to its theoretical level. However, in response to a paper by Thomsen et al. [3], Shaw conceded that the size effect would be much smaller if one also acknowledged the energy expended in deforming the final workpiece surface. The paper by Thomsen et al. [3] argued that the force intercept at zero uncut chip thickness, derived from a plot of force versus uncut chip thickness, was the force required to deform the cut workpiece surface. The conclusion that followed was that the force required for workpiece deformation, and hence, not available for chip formation, is in large part the source of the size effect. The inference drawn was that the workpiece deformation occurred under the tool after chip separation and so could be considered as separate from the shear zone. This hypothesis will be evaluated in this paper along with others.

Masuko [4] and Albrecht [5] furthered the concept of a separable force component by attempting to quantitatively identify it, with Albrecht coining the term ''ploughing force'' to describe it. Later, Albrecht [6] refined the term ''ploughing'' to consist of two parts—chip ploughing and workpiece-deformation ploughing. Ploughing in this sense referred to the extrusion of material either below the tool and into the workpiece (workpiece ploughing), or ahead of the tool or built up edge and into the chip (chip ploughing). He noted that the workpiece-ploughing component was the same as that force identified by Thomsen et al. [3] through the intercept method. Connolly and Rubenstein [7] also developed a model for ploughing based on the assumption that the material flowing under the tool, from an assumed separation point, would undergo compression in an extrusion-like process.

Wu [8] considered a separable ploughing force component to be proportional to the volume of material forced under the tool. The limitations of this approach lie in the assumption of full material recovery as well as the difficulty in determining the penetration depth required in the analysis. Endres et al. [9] refined this volume-proportional ploughing force model through a parameter estimation routine. The shortcoming of this model is that there is no guarantee of a unique solution for its parameters, making physical interpretation of results difficult.

Waldorf [10] developed a slip-line model for blunt tools that is similar to that of Abebe and Appl [11], who formulated their model for negative rake cutting. These models postulated material deformation ahead of the cutting edge as well as below the uncut chip thickness depth. Use of Waldorf's model is limited in practice due to the required a priori determination of several geometric variables that define the geometry of the slip line field. Nevertheless, these models are enlightening in that they show how deformation of material ahead of the cutting edge, yet not becoming part of the chip, may be key in understanding the impact of edge bluntness on the geometry of material deformation and the machining forces.

As seen in the above discussion, the bulk of the research on this subject has assumed that the machining force obtained using a blunt-edged tool consists of a chip formation or shearing component and a *separable* ploughing component. The magnitude of the shearing component is assumed to be identical to that which would be observed if the operation was performed using a perfectly sharp tool. Thus, the ploughing force is obtained as a difference between the measured force and the force obtained using a perfectly sharp tool (all else held constant). Approaches to assessing the ploughing force behavior, one analytical and the other

Contributed by the Manufacturing Engineering Division for publication in the JOURNAL OF MANUFACTURING SCIENCE AND ENGINEERING. Manuscript received February 1999; revised May 2001. Associate Editor: M. Elbestawi.

experimental, have appeared in the literature. Of these, the extrapolation procedure of Thomsen et al. [3], mentioned previously, is the most widely used. However, it does not enjoy universal support [12,13]. Stevenson [14] has further suggested, based on experimental evidence, that the extrapolation approach is incorrect. An experimental procedure, the feed-dwell approach, was proposed by Colwell and co-workers [15,16] and was evaluated further by Stevenson [12]. This approach considers the ploughing force to be that measured on the tool just before first forming a chip. This ploughing force can be measured directly by reducing the machine feed (i.e., decreasing the uncut chip thickness) to zero while continuing to "machine." The force measured after the chip ceases to form is then considered as the ploughing force.

In the work presented here, no presumption is made as to the physical origin of the force trends. Rather, a number of interpretations of how the observed force trends arise and how well these interpretations reflect this behavior will be explored. In order to do this objectively we adopt the criterion that any analysis conducted on blunt tool cutting must yield the same fundamental material response as would be observed with a sharp tool. Thus, we will use the known material response as an internal marker to evaluate model capability.

2 Experimental Procedure

Orthogonal machining tests were performed on 99.99 percent pure zinc received as 101.6 mm diameter continuously poured bar stock. The bar stock was turned and bored to final tube dimensions of 98.43 mm outer diameter, 5.08 mm wall thickness, and 250 mm length for orthogonal end turning tests.

2.1 Tests Conducted. Testing was initially conducted on a CNC lathe. However, during the initial stages of conducting dwell tests as described by Stevenson [12], a problem caused by controller feedback was detected. Thus, all dwell tests were performed on a manual lathe following a procedure based on randomization and replication for experimental soundness. Figure 1 shows representative force signatures of this method.

A further set of conventional orthogonal machining tests was performed on a CNC lathe at smaller feeds. In this set of tests the largest feeds replicated the smallest two feeds used in the dwell tests. The feed was reduced in a step-wise fashion every 19 workpiece revolutions. After the smallest feed was reached the feed was increased, again in a step-wise fashion (see Fig. 2), efficiently generating a large quantity of data, and allowing for the evaluation of the impact of previous feed conditions.

2.2 Experiment Conditions. Table 1 shows the levels of the variables employed in the tests. The various rake angles were achieved using individual tool holders with zero back rake and lead angles. Honed, T_G 432, uncoated carbide inserts were specially produced by a commercial tooling supplier to a variety of edge radii and relief angle to maintain a constant six-degree clearance across all rake angles. Each insert was measured to confirm the specified six-degree clearance angle and to record the true edge radius. A white-light interferometer measurement system was employed and the techniques of Schimmel et al. [17] were followed to determine the edge radius of all inserts in the cutting zone. From the population of inserts measured a set was chosen such that for each rake angle one of each of the targeted edge radii was achieved. The radii were measured again after all testing; no significant changes were found.

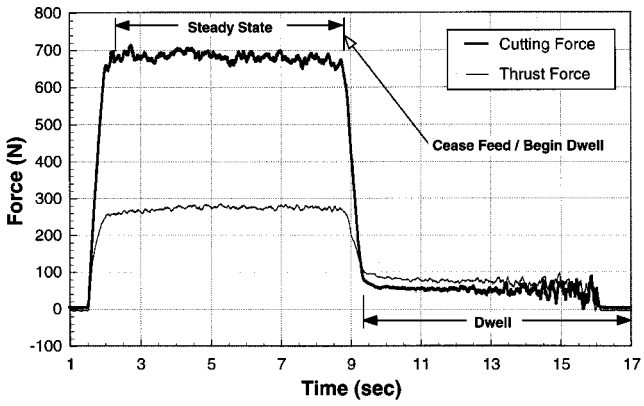

Fig. 1 Typical cutting and thrust force signatures during feed dwell tests

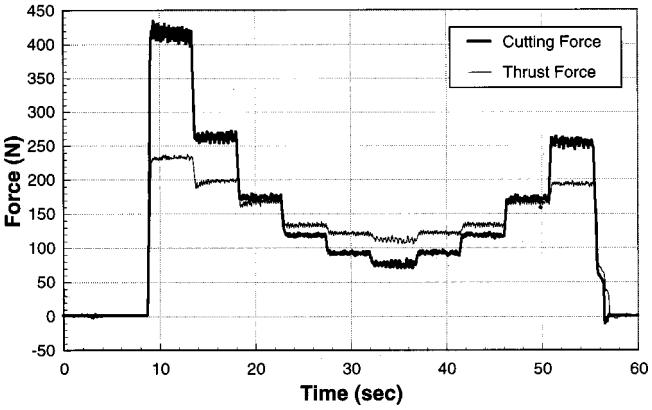

Fig. 2 Typical cutting and thrust force signatures from CNC step test

Table 1 Test Conditions (all combinations run, except r_n = 140 μm, which was run with +5 deg rake only)

Velocity (V)	0.647 (133), 1.246 (256) m/s (rpm)
Orthogonal rake angle (γ_o)	+5, 0, −16 deg
Edge radius (r_n)	0, 28, 33, 80, 140 μm
Uncut chip thickness (h)	2.9, 5.9, 11.8, 23.6, 47, 94, 186, 377 μm

2.3 Measurements. Cutting, thrust and lateral force measurements were made with a piezoelectric dynamometer and were recorded using a PC-based data acquisition system. Chip thickness measurements were made with a point micrometer. For each feed, six chip thickness measurements were made at the midwidth line and the average taken as the thickness. Even for large edge radii the side spread in the chip was small, relative to the width of cut, which indicates that near plane-strain conditions existed. A laser measurement system was used to verify the feed of the tool holder relative to the bed of the lathe. Video images were captured by a Xenon-strobe video system using a strobe rate of 30 sec^{-1} and a telephoto lens. The video images were used in identifying changes in chip contact with the rake face. The camera was mounted to move with the tool and was oriented perpendicular to the action of cutting.

2.4 Data Reduction. As noted, Fig. 1 shows the force signals from a typical dwell test. Figure 2 shows the force signals from a typical CNC step test. In all cases the sampling frequency was 512 Hz. The steady-state forces were calculated as the average force over the final five revolutions for each feed condition. In the CNC step test where the feeds were stepped down and then back up, a direct comparison could be made to check for any impact of the prior feed condition. Such comparisons showed there was no noticeable effect of the previous feed conditions on steady-state forces. The same held true for (cut) chip thickness. This confirms the work of Stevenson and Stephenson [18].

All the responses, including force components, chip thickness, and shear angle, each versus uncut chip thickness, as well as shear

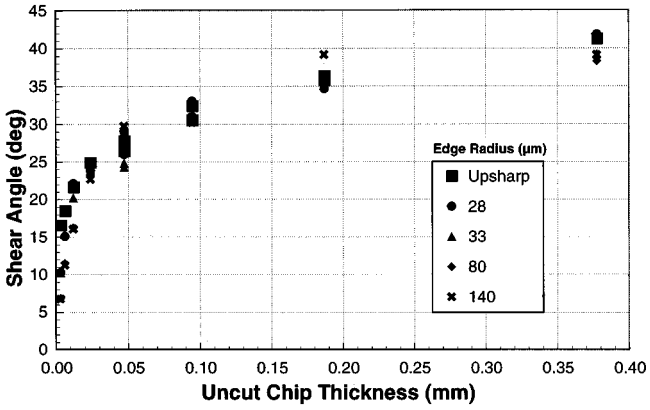

Fig. 3 Shear angle vs. uncut chip thickness (5 deg rake, 256 rpm)

stress versus strain rate, showed similar trends for each rake angle and speed combination. Hence, for the sake of brevity, most of the response data shown in the figures will be for the 1.246 m/s (256 rpm), five-degree rake angle case to present a typical result, with any exceptions noted.

Of interest in the ensuing analyses is the graph of shear stress versus strain rate. To that end, the force data must be converted to shear stress in the shear plane. The analyses differ in the details of those conversions, but in general they make use of the traditional relation

$$\tau = \frac{F_C \sin \phi_o \cos \phi_o - F_T \sin^2 \phi_o}{h \cdot w} \tag{1}$$

where w is the width of cut and h is the uncut chip thickness.

The analyses also differ in the details of how shear angle and strain rate are computed. The strain rate, $\dot{\gamma}$, is calculated according to Oxley's [19] method in which the shear zone is approximated as parallel sided with a thickness proportional to the shear-plane length. The *nominal* shear angle, denoted as ϕ_o in Eq. (1) and used to compute shear strain as well, is computed in the usual way from the chip ratio, r_h, while using the *nominal* orthogonal rake angle γ_o. The chip ratio is determined using the six-point averaged chip thickness and the commanded feed rate (h, the uncut chip thickness). Figure 3 shows the nominal shear angle versus uncut chip thickness. Figure 4 shows the cutting and thrust force data versus uncut chip thickness for that same typical set of tests.

3 An Analysis of Data Under a Sharp-Tool Assumption

The previous work of Stevenson and Stephenson [13] demonstrated that, during machining, zinc approximates visco-plastic behavior, i.e., $\tau = k\dot{\gamma}^m$, with the exponent m being dependent on temperature and, hence, cutting speed. A conventional analysis of the data is presented here where:

- The shear angle used is the nominal shear angle, which is computed using the nominal rake angle, as described above.
- The shear stress is calculated using Eq. (1).

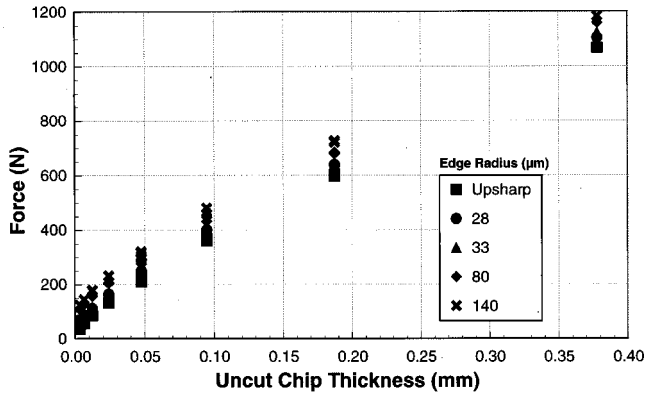

Fig. 4 Forces vs. uncut chip thickness (5 deg rake, 256 rpm): (*a*) cutting (*b*) thrust

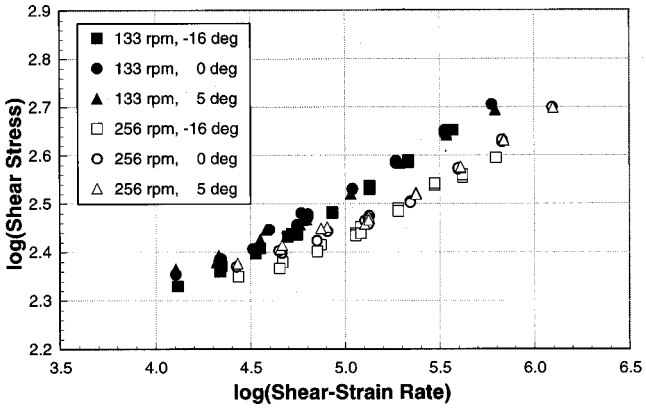

Fig. 5 Shear stress vs. shear-strain rate (log-log) for all sharp tool data

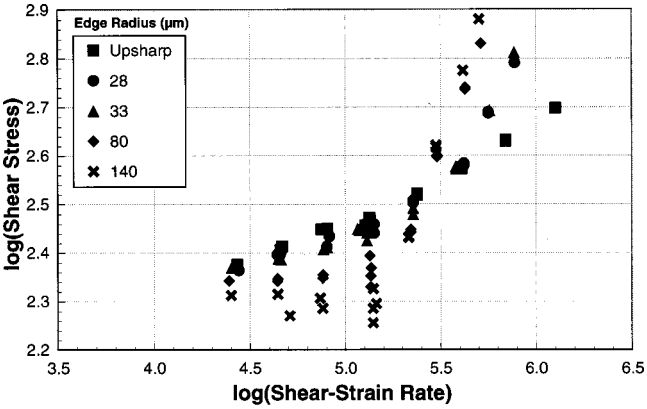

Fig. 6 Shear stress vs. shear-strain rate (log-log) across edge radii (5 deg rake, 256 rpm)

- Strain rate is computed using a shear-zone thickness of one-tenth the shear-plane length per Oxley's [19] work.

The stress and strain rate results for all sharp tools ($r_n=0$) are shown in Fig. 5. The analysis produces straight lines in the log-log space where the slope m is dependent on cutting speed, or likewise spindle speed (rpm) for the case at hand where the workpiece diameter is constant. This data set, exhibiting a straight line, confirms the assumed material model ($\tau=k\dot{\gamma}^m$).

Figure 6 shows the stress and strain rate results for all edge radii in a typical data set (five-degree rake, 256 rpm). In this plot, the blunt tools show no evidence of constant slope, unlike the case for the nominally sharp tool data in Fig. 5. The following may be observed regarding the analysis results for blunt tools:

1 At intermediate strain rates (i.e., at transitional uncut chip thicknesses) a transformation in behavior is observed, where notably different slopes are present above and below said transition.
2 In the lower strain-rate region (i.e., at large uncut chip thicknesses) the slope decreases with increasing edge radius.
3 In the higher strain rate region (i.e., at small uncut chip thicknesses) the slope increases with increasing edge radius.

The failure of this analysis is not unexpected since it is founded on the traditional assumption of sharp-edged tools. It clearly shows the inability to model the performance of blunt tools under the sharp tool assumption.

4 An Analysis Based on Previously Proposed Force Separation Methods

The separation methods are implemented by correcting the measured cutting and thrust force components, F_C and F_T, by subtracting the respective ploughing force components, F_{Cp} and F_{Tp}, to obtain the shearing (chip formation) portions as

$$F_{Cs}=F_C-F_{Cp} \quad \text{and} \quad F_{Ts}=F_T-F_{Tp}. \tag{2}$$

The shear stress is again computed in the traditional manner as in Eq. (1) but by using the shearing related force components, i.e.,

$$\tau_{\cdot}=\frac{F_{Cs}\sin\phi_o\cos\phi_o-F_{Ts}\sin^2\phi_o}{h\cdot w}, \tag{3}$$

where the $\cdot$ subscript will indicate the method used to correct for the ploughing force. As noted earlier, w is the width of cut and ϕ_o is the shear angle computed from the chip ratio using the nominal orthogonal rake angle γ_o. Strain rates were calculated as previously noted (using a shear-zone thickness of one-tenth the shear-plane length).

4.1 Dwell Forces. The first separation method employed considers the dwell forces (F_{Cd},F_{Td}) to be equivalent to the ploughing related components (F_{Cp},F_{Tp}), following Stevenson [12]. The shear related force components F_{Cs} and F_{Ts} are then calculated as

$$F_{Cs}=F_C-F_{Cd} \quad \text{and} \quad F_{Ts}=F_T-F_{Td}.$$

As shown in Fig. 7, which is typical of all dwell tests, the dwell force components are mainly a function of edge radius. However, cutting velocity (not shown) also had an effect. For each combination of insert (rake angle and edge radius) and speed, an average dwell force is calculated as an average across all feeds.

Figure 8 shows typical results for the dwell-corrected stress τ_d versus strain rate, in this case for positive five-degree and negative sixteen-degree rake angles and 256 rpm. It is clear that this

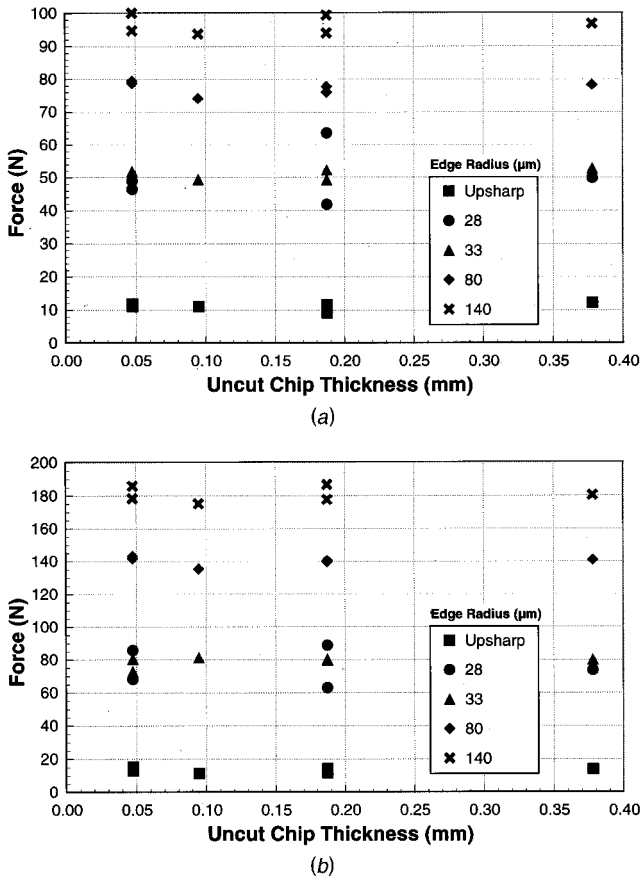

Fig. 7 Dwell forces vs. uncut chip thickness (5 deg rake, 256 rpm): (*a*) cutting F_{Cd}, (*b*) thrust F_{Td}

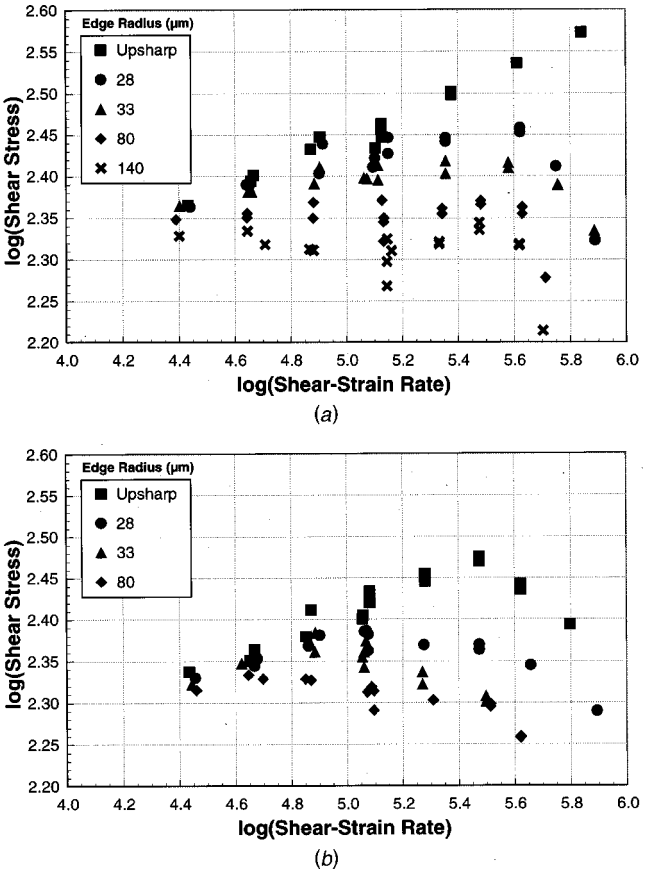

Fig. 8 Shear stress vs. shear-strain rate (log-log) for dwell-corrected nominal stress (256 rpm) at nominal rake angles of: (*a*) +5 deg (*b*) −16 deg

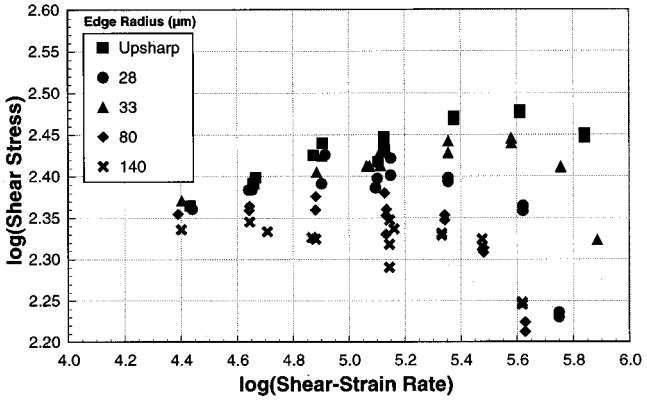

Fig. 9 Shear stress vs. shear-strain rate (log-log) for extrapolation-corrected nominal stress (5 deg rake, 256 rpm)

method fails to improve the consistency of the material response, i.e., it fails to collapse the results to those of the corresponding sharp tool. In the low strain rate region the decrease of slope with increasing edge radius became even more significant. For consistency, since the sharp tools also exhibited non-zero dwell forces the dwell-correction was applied to the nominally sharp tool data as well. In the high strain rate region, with the subtraction of a constant set of dwell components, even the sharp tool data produced in many cases an inconsistent relation (non-constant slope) between log stress and log strain rate.

The dwell-corrected approach is based on the implicit assumption that the ''ploughing mechanisms'' during dwell are the same as those during cutting, and so their associated forces are the same. The failure of this technique shows that this assumption is in error.

4.2 Zero-Feed Extrapolated Forces. The second separation method employed was to use the force graphs extrapolated to zero feed (F_{Ce},F_{Te}) as the separable ploughing components F_{Cp} and F_{Tp}, as suggested by Thomsen et al. [3]. The zero-feed force components were taken as the force-axis intercepts of second order polynomials fit to the data through the least-squared-error method. The shear related force components F_{Cs} and F_{Ts} are then calculated as

$$F_{Cs}=F_C-F_{Ce} \quad \text{and} \quad F_{Ts}=F_T-F_{Te}.$$

Figure 9 shows typical results for the extrapolation-corrected stress τ_e versus strain rate. Clearly, this method also fails to produce a consistent material response across edge radii and rake angle (the latter not shown).

5 New Analysis Method

Since neither the dwell nor the extrapolation correction techniques produce a sharp tool response from the blunt tool data, both techniques must be invalid. The new approach builds upon two assertions cited above; namely, that the shear stress is a function of strain rate only, and that the nominally sharp tool can be analyzed as ideally sharp. The first assertion may be justified by the known material behavior of zinc [13,20]. This translates to an expectation that the log stress versus log strain rate plots may be used in evaluating any proposed analysis technique—precisely the approach followed to this point. The second assertion is justified by the edge profile measurements, which showed the nominally sharp edge radii to be less than 2 μm, which is less than two-thirds of the smallest feed used. Note that in Fig. 5, the log stress versus log strain rate graphs for all the sharp-tool data sets exhibit consistent material responses with no slope changes even down to the smallest uncut chip thickness.

Three postulates on which the new analysis is based are:

1. That there is no separable ploughing force—the measured force is the deformation force and any change in force with edge radius is due to changes in the local deformation geometry.
2. That for any non-sharp tool, the shear angle derived using the nominal rake angle is incorrect when the uncut chip thickness becomes small relative to the edge radius.
3. That in the low strain rate regions of the log stress versus log strain rate plots, the decrease in slope with increase in edge radius is due to an error in the thickness assumed for the shear zone, which translates into an inversely proportional error in computed strain rate.

5.1 Justifying the Postulates. The first postulate is the basis for the overall approach.

The second postulate is conceptually reasonable (see Fig. 10) since it is straightforward to visualize different equivalent rake angles at different feeds for a blunt tool. Video images captured during cutting tests support this postulate as does the analysis proposed by Manjunathaiah and Endres [21,22]. Figure 11 shows a sequence of uncut chip thicknesses stepping from 94 μm to 2 μm all for the 80-μm edge radius, five-degree rake angle and 256 rpm combination. In these images it is evident (as highlighted with annotations for clarity) that the chip leaves the rake face closer to the shear zone as the feed decreases, and that the apparent rake angle is less than nominal. A similar postulate was advanced by Nakayama et al. [23]. Although no measurements were made from the images as the camera perspective made such direct measures unreliable, the observed trends support such a postulate.

The third postulate suggests that the actual thickness of the shear zone is something other than one-tenth the shear-plane length as suggested by Oxley for the sharp tool case. The alterna-

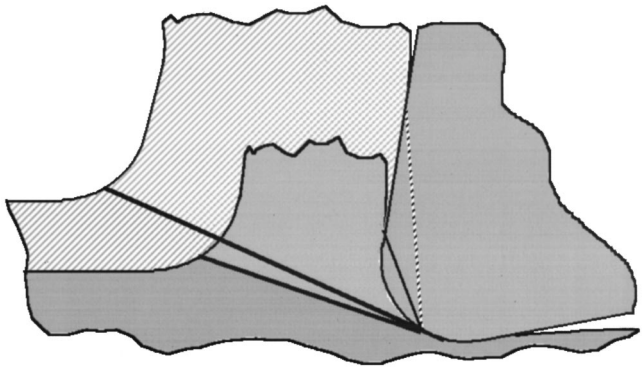

Fig. 10 Schematic of an equivalent rake angle and shear angle

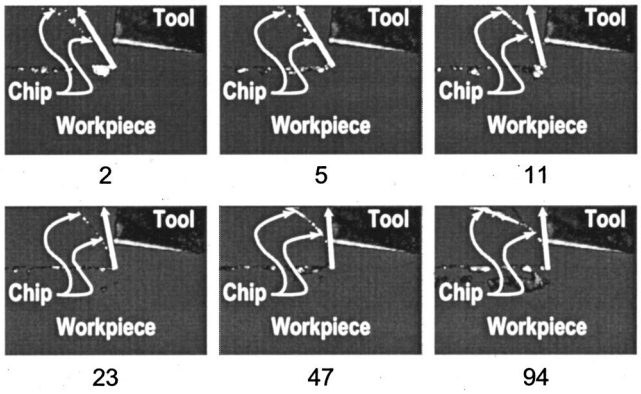

Fig. 11 Video images from CNC step test (80 μm edge radius, 5 deg rake, 256 rpm)—numeric values are the uncut chip thickness in μm, arrows indicate direction of chip departure from tool

tive presented here is that rather than 1/10, a factor $1/(10-\delta_{sz})$ can be used to describe the shear zone thickness. The parameter δ_{sz} indicates a change in shear zone thickness from the ideal sharp case, and so a positive value of δ_{sz} reflects a thickening of the shear zone. As δ_{sz} increases, the shear zone thickness increases, thereby proportionately reducing the strain rate.

5.2 Applying the Postulates. Based on the second postulate and the support provided by the video images, it is proposed that for any uncut chip thickness less than the edge radius the equivalent orthogonal rake angle $\overline{\gamma}_o$ (not to be confused with the oblique-cutting equivalent rake angle) is taken as the tangent to the edge at the point where the projection of the uncut surface intersects the edge profile. While this model is simple, for instance compared to that of Manjunathaiah and Endres [22], it provides the correct qualitative trend. Thus, assuming that the edge may have a cylindrical profile, the equivalent rake angle is

$$\overline{\gamma}_o = \begin{cases} \sin^{-1}\dfrac{h-r_n}{r_n}, & h<r_n \\ \gamma_o, & h\geqslant r_n \end{cases}. \tag{4}$$

The net effect of applying this equivalent rake angle is to decrease the computed shear angle and hence to decrease calculated values of both strain rate and shear stress. In this case the strain rate $\dot{\gamma}$ is calculated according to Oxley's [19] method with the use of the equivalent, rather than the nominal, orthogonal rake angle. Figure 12 shows the results of applying this correction to the data for the typical case, again presented as log stress versus log strain rate. The elementary assumption on equivalent rake angle calculation seems to hold quite well, with the 140 μm and 80 μm radius cases at the smallest uncut chip thickness (highest strain rate) showing the greatest deviation. These are the most extreme cases. Since the edge was modeled as a cylinder, minor deviations in actual geometry as well as minor errors in uncut chip thickness will have a significant impact on miscalculation of equivalent rake angle values and hence the calculated shear stress and strain rate. Since the geometric model makes no change in calculations when the uncut chip thickness is greater than the edge radius, the inconsistency in slope across different edge radius is still present at low strain rate (high uncut chip thickness). This remaining inconsistency is removed by applying the third postulate.

Unlike the second postulate, there is no analytical model for shear-zone thickening. Thus, an empirical approach was adopted. To estimate the thickening of the shear zone, a least squares linear fit to the log-log data of each sharp tool was made. This established a target curve. Then, the data from tools of non-zero edge radius were reanalyzed. For each edge radius, in the same rake angle-speed data set, over the range of $h>r_n$, a modified strain rate is computed as

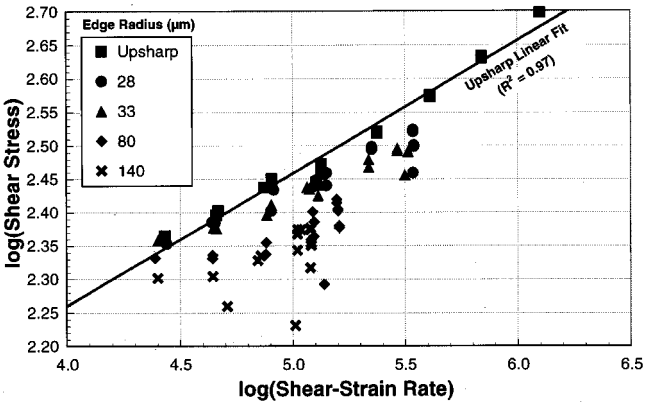

Fig. 12 Shear stress vs. shear-strain rate (log-log) for stress calculated using equivalent rake angle only (5 deg rake, 256 rpm)

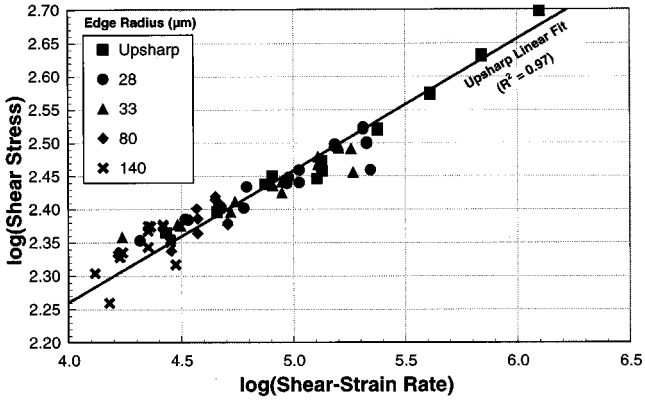

Fig. 13 Shear stress vs. shear-strain rate (log-log) for stress calculated using equivalent rake angle and shear zone thickening (5 deg rake, 256 rpm)

$$\overline{\dot{\gamma}} = \frac{\dfrac{\cos\overline{\gamma}_o}{\cos(\overline{\phi}_o-\overline{\gamma}_o)}}{\dfrac{h}{(10-\delta_{sz})\sin\overline{\phi}_o}} V, \tag{5}$$

where $\overline{\phi}_o$ is the shear angle computed using the equivalent rake angle $\overline{\gamma}_o$. The estimate for δ_{sz} was made by a least-squared-error fit between the measured sharp tool ($r_n=0$) shear stresses and the strain-rate adjusted shear stresses for each r_n. The value of δ_{sz} was then held to be a constant for a given tool and applied over all feeds in a given rake angle-speed data set. The effect on the data analysis is shown in Fig. 13 for the typical data set and is similar for all others.

5.3 Evaluating the Postulates. Regarding the third postulate, the factor δ_{sz} as estimated for all cases varied quite linearly with log of the edge radius, with slope being relatively constant across speeds for each rake angle, and slope increasing slightly with speed. Note that, for either speed, the negative sixteen-degree rake angle set has a thinner shear zone (smaller δ_{sz}) than the zero- and five-degree cases, across all edge radii. This trend in the shear-zone thickness increasing as rake angle becomes larger (positive) contradicts speculations made by Kececioglu [24] for machining of steel. Therefore, a set of quick-stop tests was performed in order to support the trends seen in this analysis. The tests were performed at 33 rpm on the manual lathe and the largest feed used in the previous dwell tests, but in this case the spindle brake was suddenly engaged while cutting.

Using high-speed video recording at 1000 frames per second, the ''quickness'' of the stopping action was evaluated. A strip of graph paper was affixed to the outer circumference of the tube so that the axially running grid lines could be tracked and the distance traveled per frame measured. By examining the video, the time at which the distance traveled by the tube per frame began to change could be identified, thus marking the beginning of stopping. The distance traveled by any convenient grid line to a full stop could then be measured. Based on Kececioglu's [24] report of his study, it is estimated that the distance traveled by the workpiece in his quick-stop tests may have been as much as two times the shear-zone thickness. The distance to stop in the current set of tests, identified as approximately 0.90 mm, is also roughly twice the average shear-zone thickness of 0.45 mm, as measured from the quick-stop micro-graphs. Therefore, the quick stop tests here are deemed comparable to those of Kececioglu.

The micro-graphs produced after the quick stops are shown in Fig. 14. The samples were electrolytically polished and tint etched and then photographed under polarized light. Due to the high

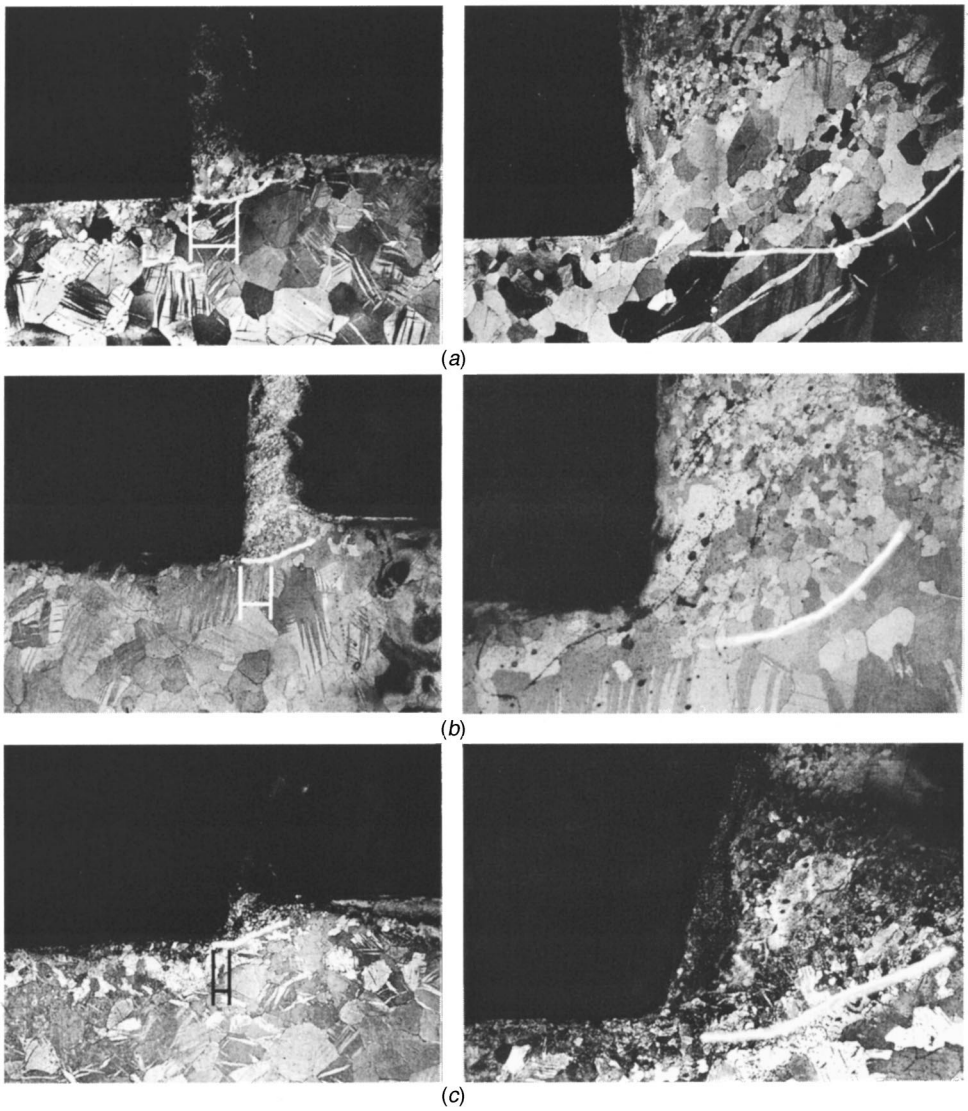

Fig. 14 Micrographs of quick stop tests for an 80 μm edge radius and a 377 μm uncut chip thickness at rake angles of: (*a*) 5 deg, (*b*) 0 deg, and (*c*) −16 deg

purity and low melting point of the zinc, a very different record of machining is produced than is typically seen. Traditionally, micrographs show a distorted grain pattern with the distortions being associated with deformation in machining. In this case, however, the micro-graphs show re-crystallization in the deformed regions, which appears as a marked decrease in grain size from the large grains associated with the as cast structure to the smaller grains associated with the areas that were experiencing deformation at the instance of the quick stop. In this way the boundary of the shear zone can be estimated. The thin recrystallized layer at the work piece surface, visible ahead of the tool in the 25× (left) figures, is due to the previous pass of the tool.

Lines denoting the boundaries of the shear zones were added to the micro-graphs to clarify the ensuing discussion. As noted, these boundaries were established by observing the change in grain size when moving from the incoming direction, through the shear zone, and then out of the primary shear zone into the chip. Comparison of the forward boundary for the three rake angles of the 80 μm tools shows that the trend inferred from the δ_{sz} model regression, which is opposite that suggested by Kececioglu [24], is supported by this data. More specifically, the five-degree rake tool clearly has a shear front extending far forward of the negative sixteen-degree rake tool meaning that the five degree rake angle produces a thicker shear zone. Therefore, although no direct quantifiable comparisons can be made since the initial cutting velocity of the quick stops is much lower than the velocities in the main study, the observed trends do support the analysis method suggested herein.

5.4 Summary. The analysis given here has shown that force separation techniques fail to provide a means of considering the effect of edge radii in metal cutting by the failure of the work material to respond in a consistent manner. However, considering an integrated view of the deformation process yielded a consistent work-material response. This integrated view led to an analysis that relies on an analytical calculation of an equivalent rake angle for conditions where uncut chip thickness is less than the edge radius, and an empirical regression to calculate the shear zone thickness. These two ''corrections'' for the presence of edge radius were applied universally and succeeded in returning a consistent material response (stress versus strain rate) across a wide range of rake angle, edge radius, uncut chip thickness and speed.

In addition to the numerical consistency, the observed trends in changes in equivalent rake angle and shear zone thickness are supported by independent experimental observation.

6 Conclusions

1. Only for sharp tools does the shear stress versus strain rate (material response) determined through cutting tests and analysis that is based on Merchant's [1] sharp-tool model show consistent trends when compared to material compression tests. The trends are inconsistent when the same sharp-tool analysis is applied for blunt tools.
2. Estimation of a separable ploughing force using the extrapolation technique of Thomsen et al. [3] fails to produce consistent material response trends regardless of the tool edge radius.
3. Estimation of a separable ploughing force using the dwell technique of Stevenson [12] fails to produce consistent material trends regardless of the tool edge radius.
4. Use of an equivalent rake angle for blunt tools when the uncut chip thickness is less than the edge radius is supported by the analysis of experimental data.
5. The suggestion that the shear zone thickness is solely related to the shear plane length is not supported for blunt edge tools. Rather, the analysis presented here shows that the shear zone thickness is some function of the shear plane length, edge radius, and cutting velocity.

Acknowledgments

The assistance of Deiter Ebner in all aspects of the experimental program, Glen Novak in edge measurement, as well as Scott Hucker and Ken Brown in data analysis, is greatly appreciated. The authors also thank Mark Gillman of General Motors for resource support. We deeply appreciate the efforts of Bill Hughes, James Kasperik and Todd Quick of Kennametal Inc. for providing the cutting inserts.

References

[1] Merchant, M. E., 1945, ''Mechanics of the Metal Cutting Process: I-Orthogonal Cutting and the Type 2 Chip,'' J. Appl. Phys., **16**, pp. 267–275.
[2] Backer, W. R., Marshall, E. R., and Shaw, M. C., 1952, ''The Size Effect in Metal Cutting,'' Trans. ASME, **74**, pp. 61–72.
[3] Thomsen, E. G., Lapsley, J. T., and Grassi, R. C., 1953, ''Deformation Work Absorbed by the Workpiece During Metal Cutting,'' Trans. ASME, **75**, pp. 591–603.
[4] Masuko, M., 1953, ''Fundamental Research on Metal Cutting (1st Report), A New Analysis of Cutting Forces,'' Trans. Jpn. Soc. Mech. Eng., **19**, pp. 32–39.
[5] Albrecht, P., 1960, ''New Developments in the Theory of Metal Cutting Process: Part I-The Ploughing Process in Metal Cutting,'' ASME J. Eng. Ind., **82**, pp. 348–357.
[6] Albrecht, P., 1961, ''New Developments in the Theory of Metal Cutting Process: Part II-The Theory of Chip Formation,'' ASME J. Eng. Ind., **83**, pp. 557–568.
[7] Connolly, R., and Rubenstein, C., 1968, ''The Mechanics of Continuous Chip Formation in Orthogonal Cutting,'' Int. J. Mach. Tool Des. Res., **8**, pp. 159–187.
[8] Wu, D. W., 1988, ''Application of a Comprehensive Dynamic Cutting Force Model to Orthogonal Wave Generating Processes,'' Int. J. Mech. Sci., **30**, pp. 581–600.
[9] Endres, W. J., Devor, R. E., and Kapoor, S. G., 1995, ''A Dual Mechanism Approach to the Prediction of Machining Forces-Parts I & 2,'' ASME J. Eng. Ind., **117**, pp. 526–542.
[10] Waldorf, D. J., 1996, ''Shearing, Ploughing and Wear in Orthogonal Machining,'' Ph.D. Thesis, University of Illinois at Urbana-Champaign.
[11] Abebe, M., and Appl, F. C., 1981, ''A Slip-Line Solution for Negative Rake Angle Cutting,'' Proc., NAMRC, **19**, pp. 341–348.
[12] Stevenson, R., 1998, ''The Measurement of Parasitic Forces in Orthogonal Cutting,'' Int. J. Mach. Tools Manuf., **38**, pp. 113–130.
[13] Stevenson, R., and Stephenson, D. A., 1995, ''The Mechanical Behavior of Zinc During Machining,'' ASME J. Eng. Ind., **117**, pp. 172–178.
[14] Stevenson, R., 1999, ''A Reassessment of the Extrapolation Technique for Determining the Parasitic Cutting Loads under Orthogonal Cutting in Strain Rate Hardening Materials,'' Mach. Sci. Technol., **3**, pp. 1.
[15] Colwell, L. V., 1971, ''Methods for Sensing the Rate of Tool Wear,'' CIRP Ann., **19**, pp. 647.
[16] Colwell, L. V., and Mazur, J. C., 1976, ''Tool Wear Tracking in the Production Shop,'' Proc., NAMRC, pp. 420.
[17] Schimmel, R. J., Manjunathaiah, J., and Endres, W. J., 2000, ''An Experimental Investigation of the Variability of Edge Hones and Their Effects on Machining Forces,'' ASME J. Manuf. Sci. Eng., **122**, pp. 590–593.
[18] Stevenson, R., and Stephenson, D. A., 1996, ''The Effect of Prior Cutting Conditions on the Shear Mechanics of Orthogonal Machining,'' ASME J. Manuf. Sci. Eng., **120**, pp. 13–20.
[19] Oxley, P. L. B., 1989, *The Mechanics of Machining: An Analytical Approach to Assessing Machinability*, Ellis Horwood Limited, Chichester.
[20] Wagoner, R. H., 1981, ''A Technique for Measuring Strain Rate Sensitivity,'' Metall. Trans. A, **12A**, pp. 71–75.
[21] Manjunathaiah, J., and Endres, W. J., 1996, ''Effects of a Honed Cutting Edge in Machining,'' Proc., Second S. M. Wu Symp. on Mfg. Sci., pp. 25–30.
[22] Manjunathaiah, J., and Endres, W. J., 2000, ''A Study of Apparent Negative Rake Angle and its Effects on Shear Angle During Orthogonal Cutting with Edge-Radiused Tools,'' Trans. NAMRI/SME, **28**, pp. 197–202.
[23] Nakayama, K., and Tamura, K., 1968, ''Size Effect in Metal Cutting Force,'' ASME J. Eng. Ind., **90**, pp. 119–126.
[24] Kececioglu, D., 1958, ''Shear-Strain Rate in Metal Cutting and its Effects on Shear-Flow Stress,'' Trans. ASME, **80**, pp. 158–168.